Math. Model. Nat. Phenom. 13 (2018) 52
https://doi.org/10.1051/mmnp/2018056

**Mathematical Modelling of Natural Phenomena**
www.mmnp-journal.org

# MULTIPLE COMBUSTION REGIMES AND PERFORMANCE OF A COUNTER-FLOW MICROCOMBUSTOR WITH POWER EXTRACTION

E. Fernández-Tarrazo[1,*], M. Sánchez-Sanz[1], R. Fursenko[2] and S. Minaev[3]

**Abstract.** Power generation usually requires removal of thermal energy from the system. In this paper, we evaluate the impact of the heat removal on the dynamics of a premixed flame in the case of a simple, but representative, counter-current microburner. In this configuration, two opposed streams of fresh gases with the same equivalence ratio $\phi$ are introduced, at the same velocity $U_{\mathrm{F}}$, in the burner through narrow, infinitely long channels. The channels are separated by the common wall from which the heat used for power generation is removed. A flame-sheet chemistry model and a realistic, specifically developed, one-step Arrhenius kinetics are used and compared in order to explore the importance of finite-rate chemistry effects. Finite-rate is found to play a significant role especially near the extinction limit (low velocities) and at high temperatures (high velocities) where distributed reaction can lead to autoignition. The changes in the flame stabilization position and operation limits of the burner are analyzed. Significant variations in combustor operation were found when energy is extracted from the system. Power generation efficiency is also studied, to conclude that an optimum level of energy extraction exists for each equivalence ratio and also that an optimum equivalence ratio exists.

**Mathematics Subject Classification.** 80A20, 80A32

Received April 6, 2018. Accepted September 20, 2018.

## 1. Introduction

Micro-combustion is characterized by a sequence of exothermic reactions between a fuel and an oxydizer that occurs in special devices (microcombustors) with a characteristic scale of the order of the thermal thickness $\delta_{\mathrm{L}} = D_{\mathrm{T}}/V_{\mathrm{L}}$, where $D_{\mathrm{T}}$ and $V_{\mathrm{L}}$ are, respectively, the thermal diffusivity and the flame propagation velocity. One of the major problems with the usage of micro-combustors is the flame extinction due to heat loss at the walls. As the size of the system decreases, the ratio area/volume increases, and heat loss leads to the flame extinction, a fact early recognized by Davy [1].

*Keywords and phrases:* Micro-combustion, counter-current microcombustor, heat recirculation, methane flame.

[1] Department y de Fluidos, Universidad Carlos III de Madrid, Leganés 28911, Spain.
[2] ITAM SB RAS, Novosibirsk, 630090, Russia and Far Eastern Federal University, Vladivostok 690090, Russia.
[3] Far Eastern Federal University, Vladivostok 690090, Russia.

* Corresponding author: eafernan@ing.uc3m.es

Article published by EDP Sciences

© EDP Sciences, 2018

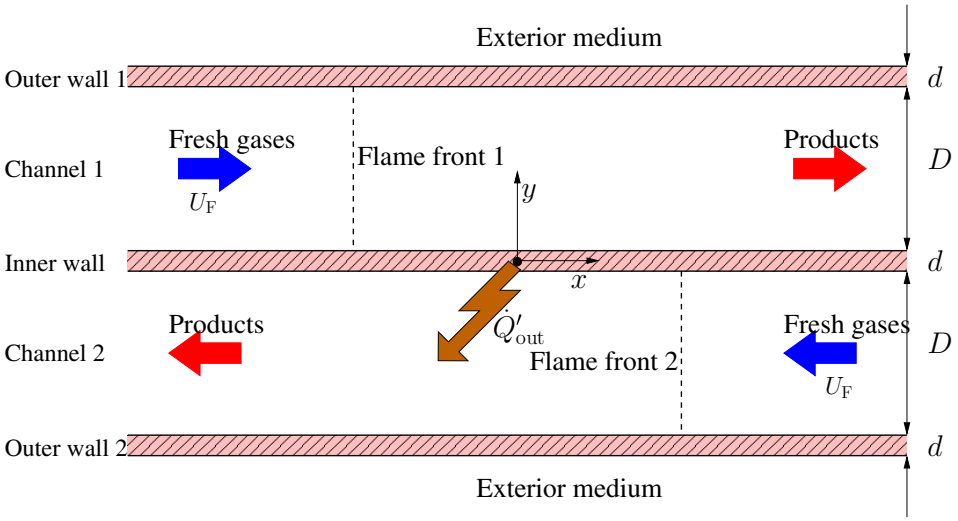


FIGURE 1. Counter-flow microburner sketch.

While heat transfer to the walls is large in micro-combustors, this heat can be recirculated to pre-heat the incoming fresh gases before combustion [24]. Preheating produces superadiabatic combustion temperatures and extends flammability limits [6, 7, 22], which can be used to increase the system efficiency.

Micro-combustion of liquid fuels – and subsequent thermal energy conversion – is an alternative to electric batteries portable power source, due to the high energy density of liquid fuels compared with batteries. Estimates [3] suggest that a microgenerator with a global efficiency on the order of 2% would be competitive with the available state-of-the-art batteries, in terms of energy density.

Among the numerous attempts to scale micro-engines down to the meso-scale we could mention a micro gas-turbine engine [2] and a micro rotative engine [5]. A number of reviews on micro-combustion can be found in the literature [3, 9, 10].

Experience with scaled-down systems suggests that more fundamental research is needed in understanding and developing devices to generate portable energy. Much research has been conducted on the combustion characteristics in such micro-combustors [17–20] and energy production [11, 15, 16], but little work has been carried out on the interaction of the combustion with the removal of energy from the system. If the amount of energy extracted from the system is significant, the temperature distribution will change, producing a potentially large effect on the flame dynamics, especially near the flammability limit. Consequently, the combustor operation and performance will also be affected by the extraction of energy.

In this work we will analyze the counter-flow microburner shown schematically in Figure 1. It is a simple yet representative microburner, similar to the one considered by Fursenko and Minaev [6, 7]. This is a well-known configuration where we will introduce the effect of heat removal $\dot{Q}'_{out}$ to analyze the effects on flame dynamics and combustor operation. In order to keep small the number of parameters, we will consider the thermal energy removal $\dot{Q}'_{out}$ to occur at a single point, in the center of the system, that will behave as a heat sink.

In this configuration, two opposed streams of fresh gases – a mixture of methane and air – with the same equivalence ratio $\phi$ are introduced, at the same velocity $U_F$, in the burner through the narrow, infinitely long channels 1 and 2, respectively, of width $D$. The channels are separated by the common inner wall, and from the exterior medium by two outer walls. The streams can exchange heat with the heat-conducting walls, thereby allowing the exchange of energy between both streams and heat losses to the exterior medium through the outer walls.

Two steady flame fronts form after ignition and the subsequent transient evolution in both channels. Downstream from each flame front, the hot gases exchange heat with the common inner wall and with its respective

outer wall. As a result, a part of the heat released in the combustion is lost to the exterior medium and another part is used to heat the unburnt fresh gases in the other channel. The configuration is symmetrical, so that both streams of fresh gases are preheated upstream of their respective flame fronts which can, as a consequence, propagate at a larger velocity, increasing both the flammability limits and the flame temperature.

We will characterize the combustor performance in terms of the efficiency $\eta$ of the conversion of the chemical energy contained in the fuel into useful work. We will consider the conversion of the extracted heat $\dot{Q}'_{\rm out}$ into useful work to be achieved by a generic device whose efficiency will be accounted for as the Carnot efficiency $\eta_{\rm c} = 1 - T_{\rm iw}(0)/T_0$, in terms of the ambient and the extraction point temperatures, $T_0$ and $T_{\rm iw}(0)$, respectively. The global energy conversion efficiency is, therefore, given by

$$\eta = \eta_{\rm th} \times \eta_{\rm c} = \frac{\dot{Q}'_{\rm out}}{2\rho_F U_F Y_F D Q} \times \left(1 - \frac{T_{\rm iw}(0)}{T_0}\right), \tag{1.1}$$

where $\eta_{\rm th}$ is the thermal efficiency or the fraction of energy extracted from the total chemical energy available in the fresh gases and $2\rho_F U_F Y_F D Q$ is the flux per unit length of chemical energy introduced in the system.

Energy conversion can be realized in thermoelectrical or photovoltaic devices, with a conversion efficiency lower than $\eta_{\rm c}$ and, therefore, this work will provide reasonable upper-limit estimates of the energy conversion efficiency and operating limits that can be expected in such systems. The configuration considered herein is intended to be a simple one with few parameters. More efficient configurations for energy conversion can be designed but we can expect the general trends obtained here to be similar in other system layouts.

We shall use a one-dimensional formulation of the problem as a step to characterize the effects of heat extraction on the operation of this type of burners, to evaluate the performance and to increase the understanding of the operating regimes of these micro-burners. The problem so formulated should give reasonable results as long as the channel is narrow enough for the flame fronts to remain planar and the channels walls are sufficiently thin. In any case, the operating conditions of interest for real burners should be further explored with experiments and multidimensional models.

## 2. Formulation

The mathematical formulation of the problem described above requires the conservation of mass, species and energy equations in the gas phase coupled with the energy conservation equation in the solid phase. Because of the symmetry of the problem, only the gas flow in channel 1 and the temperature distributions along the inner wall and outer wall 1, $T_{\rm iw}$ and $T_{\rm ow}$, respectively, need to be solved. For the sake of completeness, the problem is formulated including the unsteady terms in the equations, even though we will only search for steady solutions.

### 2.1. Equations

The conservation equations for the gas phase, using the isobaric approximation, can be written as

$$\frac{\partial \rho}{\partial t} + \frac{\partial}{\partial x}(\rho u) = 0, \tag{2.1}$$

$$\frac{\partial \rho h}{\partial t} + \frac{\partial}{\partial x}(\rho u h) = -\frac{\partial}{\partial x}(q) - \frac{\dot{q}''_{\rm iw}(x) + \dot{q}''_{\rm ow}(x)}{D}, \tag{2.2}$$

$$\frac{\partial \rho Y_i}{\partial t} + \frac{\partial}{\partial x}(\rho u Y_i) = -\frac{\partial}{\partial x}(J_i) + \omega_i,\ i = 1, \ldots N-1, \tag{2.3}$$

where $\rho$ and $u$ are the gas phase density and velocity, respectively, and $Y_i$ is the mass fraction of species $i$. Equations (2.1)–(2.3) need to be complemented with the state equation,

$$\frac{\rho T}{W} = \frac{\rho_0 T_0}{W_0}, \tag{2.4}$$

and the thermodynamic relation between the enthalpy $h$ and the temperature $T$, given by the NASA polynomials [13]. In equation (2.4), $W$ is the average mole mass of the mixture, obtained from the relation

$$\frac{1}{W} = \sum_i \frac{Y_i}{W_i}, \tag{2.5}$$

in terms of the mass fractions $Y_i$ and mole mass $W_i$ of the species $i$.

The heat flux in the gas phase $q$ is obtained using Fourier's law, generalized to include Dufour effect,

$$q = -k\frac{\partial T}{\partial x} + \sum_i J_i h_i, \tag{2.6}$$

the $i$th species mass flux $J_i$, due to molecular diffusion, is given by Fick's law,

$$J_i = -\rho D_i \frac{\partial Y_i}{\partial x}, \tag{2.7}$$

and $\omega_i$ is the mass production of species $i$, given by the chemistry model described below.

In equations (2.6) and (2.7), the thermal conductivity $k$ and the species mass diffusivities $D_i$ are obtained using the simplified transport model developed by Smooke and Giovangigli [23], known to provide excellent results for lean methane–air mixtures.

The boundary conditions are given by

$$x \to -\infty : T = T_0;\ u = U_F;\ Y_i = Y_{i_0},\ i = 1, \dots N, \tag{2.8}$$

$$x \to \infty : \frac{\partial T}{\partial x} = \frac{\partial Y_i}{\partial x} = 0,\ i = 1, \dots N. \tag{2.9}$$

The general problem requires to solve the energy equation for the solid walls coupled with the gas phase equations (2.1)–(2.9), where the heat conduction across and along the solid walls plays a significant role in the flame stabilization process. We will consider the case of thin inner and outer walls, where the temperature variations across the walls are neglected, while the heat conduction along the solid walls is retained. Therefore, energy conservation for the thermally thin inner and outer walls requires

$$\rho_{\rm w} c_{\rm w} \frac{\partial T_{\rm iw}}{\partial t} = \frac{\partial}{\partial x}\left(k_{\rm w}\frac{\partial T_{\rm iw}}{\partial x}\right) + \frac{\dot{q}''_{\rm iw}(x) + \dot{q}''_{\rm iw}(-x)}{d}, \tag{2.10}$$

$$\rho_{\rm w} c_{\rm w} \frac{\partial T_{\rm ow}}{\partial t} = \frac{\partial}{\partial x}\left(k_{\rm w}\frac{\partial T_{\rm ow}}{\partial x}\right) + \frac{\dot{q}''_{\rm ow}(x) - \dot{q}''_{\rm L}(x)}{d}, \tag{2.11}$$

where $\rho_{\rm w}$, $c_{\rm w}$ and $k_{\rm w}$ are the wall material density, heat capacity and heat conductivity, respectively.

Equations (2.10) and (2.11) must be solved with the boundary conditions

$$x \to \pm\infty : T_{\rm iw} = T_{\rm ow} = T_0, \tag{2.12}$$

$$x = 0 : k_{\rm w}\frac{\partial T_{\rm iw}}{\partial x}\bigg|_{x=0^+} - k_{\rm w}\frac{\partial T_{\rm iw}}{\partial x}\bigg|_{x=0^-} = \frac{\dot{Q}'_{\rm out}}{d}. \tag{2.13}$$

Heat extraction at the origin, which acts as a heat sink, is reflected in a temperature minimum at that point with a jump in the temperature gradient given by equation (2.13). All simulations below have been carried out at constant levels of heat extraction. More accurate results can be obtained if detailed modeling of the heat-extracting device is introduced in the analysis.

Thermal coupling between the gas phase and the walls is given by the heat transfer terms, modelled here as

$$\dot{q}''_{\rm iw}(x) = h_{\rm i}\left(T(x) - T_{\rm iw}(x)\right), \tag{2.14}$$
$$\dot{q}''_{\rm ow}(x) = h_{\rm i}\left(T(x) - T_{\rm ow}(x)\right), \tag{2.15}$$

and the heat losses from the outer wall to the ambient is taken as

$$\dot{q}''_{\rm L}(x) = h_{\rm o}\left(T_{\rm ow}(x) - T_0\right). \tag{2.16}$$

In equations (2.14)–(2.16), $h_{\rm i}$ y $h_{\rm o}$ are the heat transfer coefficients. Taking into account the typical Reynolds and Nusselt numbers ($Re = \mathcal{O}(10^2)$ and $Nu = \mathcal{O}(1)$, respectively), involved in this type of flows [8], a realistic constant value for $h_{\rm i} = 50\,{\rm W/m^2K}$ has been considered. The heat losses to the ambient can be modified within certain limits, depending on combustor design and ambient conditions. A realistic value $h_{\rm o} = 12\,{\rm W/m^2K}$ will be used here [8].

Notice that solution of equations (2.10) and (2.11) can be avoided if adiabatic or isothermal walls are considered – which is not convenient for microcombustors –, or if the limit $d \to 0$ is taken in equations (2.10) and (2.11) (see for instance references [6, 7]); in this case walls temperature distributions are obtained explicitly as a weighted average of gas temperatures, obtained from equations (2.10) and (2.11) and (2.14)–(2.16). The results are qualitatively similar but quantitatively significant variations in the results were found and, therefore, equations (2.10) and (2.11) were retained in the analysis. At the same time, the main novelty of the present study is the accounting for heat extraction for energy conversion and mutual influence of combustion and power generation.

For the combustor geometry, we will consider $D = 2$ mm and, in order to reduce the number of parameters in the analysis, all walls are considered herein to have the same thickness $d = 1$ mm and to be made of quartz. Constant representative values for the walls properties are taken for density $\rho_{\rm w} = 2.2 \times 10^3$ kg/m$^3$, thermal capacity $c_{\rm w} = 964$ J/kg K and thermal conductivity $k_{\rm w} = 1.67$ W/m K.

## 2.2. The chemistry model

We will consider two chemistry models: the simplest one is a flame-sheet model where the reaction is taken as a Dirac delta function at the flame location similar to that used by Fursenko *et at.* [6]. Since flammability limits are important in the operation of this type of burner, as shown below, a simple, one-step irreversible Arrhenius kinetics chemistry model was developed in order to reproduce adequately the flame propagation velocities and flammability limits of methane-air flames. This one step model is an *ad-hoc* modification of the one developed by Fernández-Tarrazo *et al.* [4], where chemistry parameters were slightly modified from the original mechanism in order to better take into account recent experimental results near the lean flammability limit. No intent was made for further optimization.

In this model, the reaction proceeds according to $CH_4 + 2O_2 \to CO_2 + 2H_2O$, with a reaction rate given by an Arrhenius-type relation

$$\omega = B\left(\frac{\rho Y_{\rm CH_4}}{W_{\rm CH_4}}\right)\left(\frac{\rho Y_{\rm O_2}}{W_{\rm O_2}}\right)e^{-Ta/T}, \tag{2.17}$$

where the activation temperature $T_{\rm a}$ is a function of the equivalence ratio of the fresh gases $\phi = 4Y_{\rm CH_4,0}/Y_{\rm O_2,0}$ that, for the lean flames near the flammability limit considered herein is given by

$$T_a = T_{a_0}\left(1 + 8.250 \times (0.64 - \phi)^2\right), \ \phi < 0.64. \tag{2.18}$$

In the above expressions, $T_{a_0} = 2 \times 10^4$ K and $B = 5.5 \times 10^{15}{\rm cm^3/mol \cdot s}$. The heat released by the combustion of the unit mass of methane is given by $Q = 5.016 \times 10^7$ J/kg.

For the numerical solution of the system (2.1)–(2.18), the equations are discretized using standard second-order finite differences and a pseudo-transient iterative solution is used until convergence is achieved. The solution is found taking $U_{\rm F}$, equivalent to mass flow rate at the entrance, and $\dot{Q}'_{\rm out}$ as parameters. We will search for steady solutions of the problem defined by equations (2.1)–(2.18). In particular, once the incoming velocity of the fresh gases is defined, the flame position $x_{\rm f}$ will be determined. Here, we define the flame position $x_{\rm f}$ as the point with the maximum reaction rate, as defined by equation (2.17).

## 3. Numerical Results

Analytical results from a simplified version of model (2.1)–(2.18) for the case of a flame-sheet chemistry model were obtained by Minaev [14]. In this section, results obtained from detailed numerical integration of equations (2.1)–(2.18) are shown. Although simulations were carried out for a wide range of equivalence ratios and heat transfer coefficients, we will restrict this presentation to a fixed micro-combustor design, specified above, operating at relatively small equivalence ratios close to the flammability limit.

Fursenko *et al.* [6] showed the existence of multiple solutions and two possible types of flames when $\dot{Q}'_{\rm out} = 0$. When the heat losses are large enough, the flame can only exist within a finite distance from the origin and it can be termed as an *attached flame*. When, on the other hand, the heat losses are small enough the flame can be stabilized at any position from the symmetry plane depending on the gas flow velocity and, for a specific $U_{\rm F}$, the flame propagates without bounds along the duct. This flame can be termed as a *free flame*. These types of flames are also found when heat removal is also taken into account, $\dot{Q}'$out $\neq 0$.

### 3.1. The attached flame regime

In Figure 2, operation and performance curves of the microburner for *attached flames*, obtained here for $\phi = 0.50$, are shown for different levels of heat extraction $\dot{Q}'_{\rm out}$. The blue dashed lines correspond to simulations carried out with a flame-sheet model where chemical reaction is taken as a Dirac delta function at the flame location, similar to that used by Fursenko *et al.* [6]. In the course of the flame-sheet model simulations, it was found that the usual first-order formula for flame propagation velocity $V_{\rm L}$, based on large activation energy asymptotics [25], is not accurate enough for the realistic values of the chemical parameters given above, as the effective Zeldovich $\beta = T_{\rm a}(T_{\rm b} - T_0)/T_{\rm b}^2$ is not sufficiently large because the non-reacted gases can be significatively preheated as they approach the reaction zone. For best agreement with detailed simulations, in this flame-sheet model we choose to use the exact flame propagation velocity $V_L$, obtained numerically from the adiabatic planar flame propagation problem at different fresh gases temperatures [21]. In Figure 2a, reasonable agreement between flame-sheet and finite-rate chemistry models is shown in the regions where the reaction rate is confined to a thin region.

The plot $x_{\rm f}$ vs. $U_{\rm F}$ shown in Figure 3a is symmetric about the $x$ axis for $\dot{Q}'_{\rm out} = 0$ while a slight asymmetry can be observed as $\dot{Q}'_{\rm out}$ increases when the flame-sheet model is used, as shown in Figure 2a by the blue dashed lines.

In this work, direct comparisons with the finite-rate chemistry model are carried out. Results from simulations carried out with the finite-rate chemistry model (2.17), (2.18) are also shown, in red solid lines, in Figure 2. In this case with finite-rate chemistry, the asymmetry in the flame position curves is more pronounced. The difference between both chemistry models in terms of flame temperature $T_{\rm f}$ and wall temperature at the heat extraction point $T_{\rm iw}(0)$ is shown in Figure 2b. Flame temperature is independent of $U_{\rm F}$ when the flame-sheet model is used, regardless of $\dot{Q}'_{\rm out}$, while small variations are found when finite-rate effects are retained in the analysis. The efficiency $\eta$, however, is reasonably coincident in both models, as shown in Figure 2c. This figure shows, in particular, that an optimum level of heat extraction exists in terms of system efficiency, when the micro-combustor operates at a given equivalence ratio $\phi$.

Differences in flame structure between the flame-sheet and the finite-rate chemistry models are shown in Figure 3. In this figure, we plot the solutions along the curves without heat extraction ($\dot{Q}'_{\rm out} = 0$) in Figure 2, corresponding to points labeled $A$, $B$, $C$ and $D$. Notice the significant chemical reaction effects upstream of the

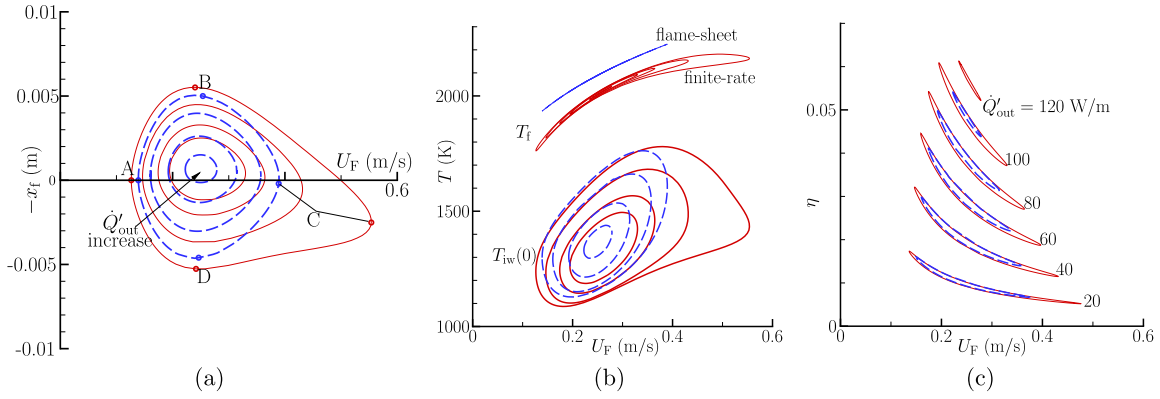


FIGURE 2. Microburner operation and performance curves for $\phi = 0.50$ for $\dot{Q}'_{\text{out}} = (0, 40, 80, 100)$ W/m. The blue dotted lines and the red solid lines correspond to the flame-sheet model and finite rate chemistry, respectively. (a) Flame position $x_f$ as a function of $U_F$. (b) Flame temperature $T_f$ and wall temperature at the heat-extraction point $T_{iw}(0)$. (c) Efficiency $\eta$ as defined by equation (1.1).

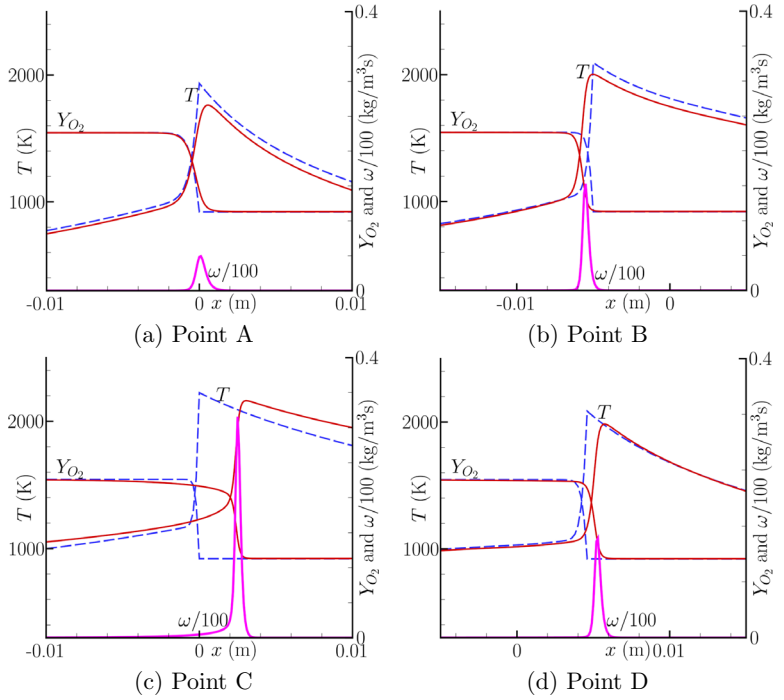


FIGURE 3. Structure of the solution at points specified as A, B, C and D in Figure 2 without heat extraction $\dot{Q}'_{\text{out}} = 0$. The dashed lines and solid lines correspond to the flame-sheet model and finite-rate chemistry model, respectively.

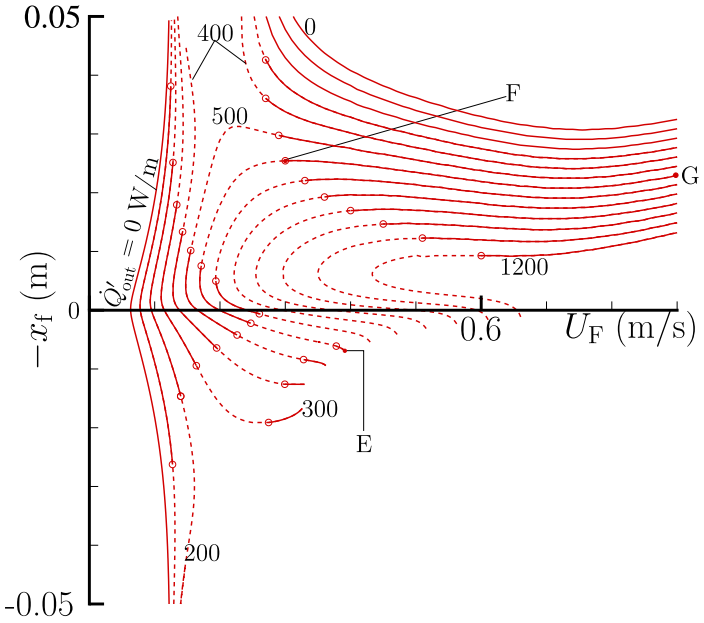


FIGURE 4. Flame position $x_f$, for $\phi = 0.58$, as a function of $U_F$ for $\dot{Q}'_{out}$ from 0 to 1200 W/m at increments $\Delta\dot{Q}'_{out} = 100$ W/m. Solid lines correspond to physical solutions while unphysical ($T_{wi}(0) < T_0$) solutions are indicated with dashed lines; the transition between these solutions is indicated with hollow circles.

flame front when $U_F$ is large (Fig. 3c). As a consequence, some oxygen consumption takes place upstream of the flame while the effect on the temperature profiles is masked by the heat transfer to the walls.

### 3.2. The free flame regime

In the *free flame* regime, the flame can be stabilized at any position in the channel, or freely propagate along the duct, depending on the fresh gases velocity $U_F$. Such regime can be realized by either reducing the heat losses or using higher equivalence ratios. In this section, we maintain the burner parameters and larger equivalence ratios are considered. Because of the higher equivalence ratio, the flame temperatures are higher and, as shown below, finite-rate effects are even more important. For this reason, in this section we will discuss only results obtained with the finite-rate model. In particular, in Figures 4 and 5, we show results for $\phi = 0.58$.

If the heat extraction is below a critical value $\dot{Q}'_{out,c}$ (between 400 and 500 W/m for $\phi = 0.58$), a freely propagating flame exists for a critical value of the fresh gases velocity $U_{F,c}$. This solution corresponds to the vertical asymptote in Figure 4 at $U_{F,c} \simeq 0.2$ m/s. In this *free-flame* regime, this asymptote separates two unconnected branches of solutions, as described by Fursenko and Minaev [7] for the case $\dot{Q}'_{out} = 0$. When heat is removed from the system for power production, these two branches are found for $\dot{Q}'_{out} < \dot{Q}'_{out,c}$ (see Fig. 4).

When the heat extracted from the system exceeds $\dot{Q}'_{out,c}$, the vertical asymptote for flame position does not exist and a single curve is obtained (see, in Fig. 4, the curves for $Q'_{out} \geq 500$ W/m ).

Notice that the curves are obtained with constant levels of heat extraction $\dot{Q}'_{out}$. When the heat extracted from the system and the flame distance $x_f$ are sufficiently large, the temperature at the origin $T_{iw}(0)$ can drop below the ambient temperature. Such solutions, shown in dashed lines in Figure 4, are ruled out as non-physical, even though they are mathematically correct. Physically meaningful solutions are represented in Figure 4 by solid lines, while non-physical solutions are are shown in dashed lines. The boundaries between them are indicated with hollow circles. Non-physical solutions are shown in Figure 4 as they clarify how the

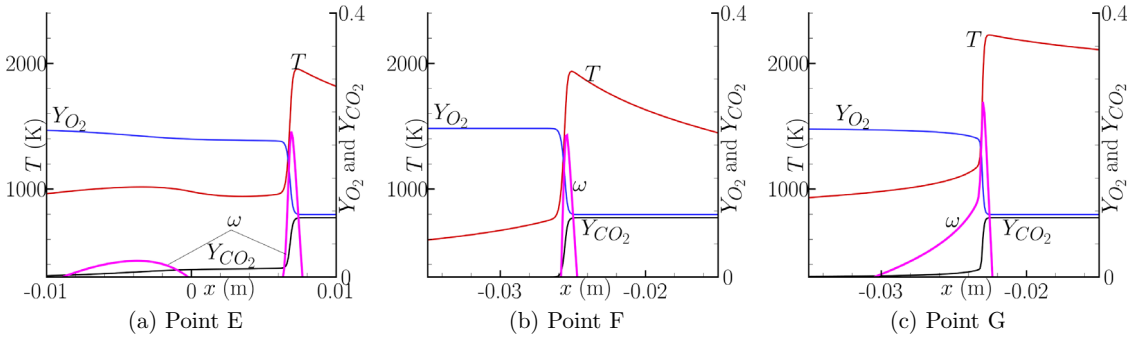


(a) Point E (b) Point F (c) Point G

FIGURE 5. Structure of the solution, for $\phi = 0.58$, at points specified as $E$, $F$ and $G$ along the curve $\dot{Q}'_{\text{out}} = 600$ W/m in Figure 2. The reaction rate $\omega$ is shown in the insets, in logarithmc scale, for illustrative purposes only.

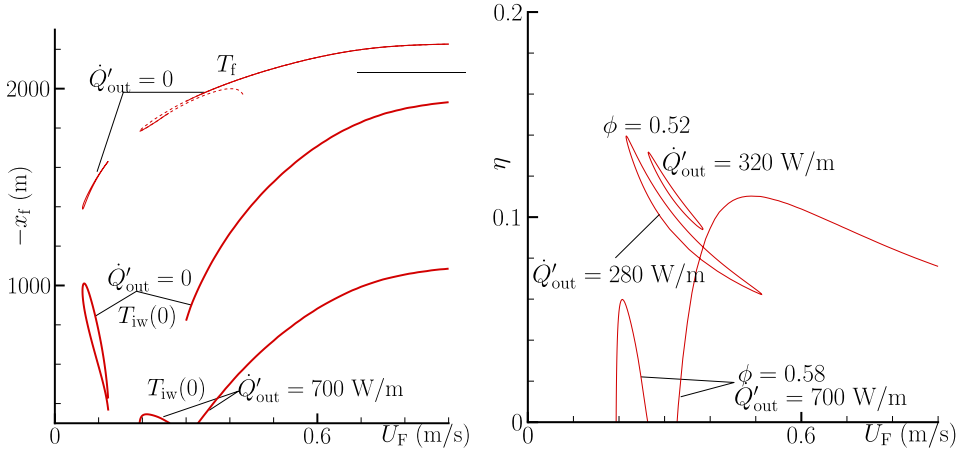


(a) (b)

FIGURE 6. (a) Flame temperature $T_{\text{f}}$ and wall temperatures $T_{\text{iw}}(0)$ at the heat extraction point. (b) Efficiency $\eta$ for $\phi = 0.58, \dot{Q}'_{\text{out}} = 700$ W/m, close to the optimum, and for $\phi = 0.52$ and $\dot{Q}'_{\text{out}} = 280$ and 320 W/m.

physical solutions branches are connected. Also, since a continuation algorithm is used, the evaluation of these solutions is helpful to find the different branches of unstable – but physically meaningful – solutions.

Three regions of physically meaningful solutions were found, as shown in Figure 4: a high speed region, a low speed region and a small, marginal region. The structure of the solutions at different representative conditions ($E$, $F$ and $G$ as labeled in Fig. 4) along the curve for $\dot{Q}'_{\text{out}} = 600$ W/m are shown in Figure 5. Notice the effects of distributed reaction for points with higher $U_{\text{F}}$ (points $E$ and $G$), while in the case of the solutions corresponding to point $F$, chemical reaction occcurs essentially in a thin reaction zone. In the case of this *free flame* regime, no limits were found in the operation for large values of $U_{\text{F}}$. As $U_{\text{F}}$ increases the temperature grows and distributed reaction upstream of the flame becomes increasingly important. Therefore, flame position cannot be determined based on flame propagation velocity alone.

In the marginal region, represented by point $E$ in Figure 4, solutions could not be obtained at higher values for $U_{\text{F}}$ because it was found that self-ignition, produced at the first maximum of gas temperature (see the corresponding flame structure at Fig. 5a) drives the flame to a radically different position. By contrast, in the case of point $G$, where distributed reaction plays an increasing role in the flame stabilization position,

the temperature profile upstream of the flame is monotonically increasing. In this case, self-ignition allows solutions with ever-increasing $U_F$. For points $E$ and $G$, the effect of distributed reaction is illustrated by the $CO_2$ concentration profiles upstream of the main reaction zone.

The flame temperature $T_f$ and the temperature at the origin $T_{iw}(0)$ are shown in Figure 6a. Notice the two unconnected regions for $\dot{Q}'_{out} = 0$, while for $\dot{Q}'_{out} = 700$ W/m the two lobes of $T_{iw}(0)$ are connected by an unphysical portion of the curve (not shown in the figure) with $T_{iw}(0) < T_0$.

The combustor efficiency can be seen in Figure 2c, for *attached flames* ($\phi = 0.50$), and in Figure 6b for *free flames* ($\phi = 0.52$ and $\phi = 0.58$). In the case of the *attached flame* regime (Fig. 2c), smooth and connected curves are obtained and the maximum efficiency is obtained at the low velocity limit. This part of the curve is likely to be unstable according to the analysis by Fursenko and Minaev [7] for a case without heat extraction and simpler physics. In the *free-flame* regime, by contrast, the existence of several physically meaningful branches correspond to several efficiency curves (connected by unphysical solutions with $\eta < 0$). In Figure 6b, the efficiency for $\phi = 0.58$ along the curve $\dot{Q}'_{out} = 700$ W/m – close to the optimum – is shown. In this case two maxima appear.

In Figure 6b, we also show the efficiency, for $\phi = 0.52$, at heat extraction levels close to the optimum, to illustrate the existence of an optimum heat extraction level and, furthermore, to show that the system can be operated more efficiently at $\phi = 0.52$ than at $\phi = 0.58$, implying the existence of an optimum equivalence ratio for this combustor. For $\phi = 0.52$, the flame was found to be *attached* but, as in the case for $\phi = 0.58$, no limit for high $U_F$ was found for small enough heat extraction.

## 4. Conclusions

Numerical simulations have been carried out for a microburner, including realistic chemistry effects and taking into account heat transfer within the walls and heat losses to the ambient. The existence of multiple solutions has been confirmed and the effect of equivalence ratio on the performance of the combustor has been analyzed. This type of analysis is of interest in order to estimate attainable efficiency and to identify operational limits and interesting regimes to be used in micro-combustor operation.

It has been confirmed that heat recirculation increases the range of equivalence ratios where micro-combustor-operation is possible, even when heat losses are taken into account [20]. Energy can be extracted from the system operating at equivalence ratios lower than 0.5. For a given microcombustor operating with a fixed $\phi$, an optimum heat extraction level $\dot{Q}'_{out}$ exists. For a given microcombustor – characterized by its geometry and external heat losses – an optimum equivalence ratio exists. For the micro-combustor under analysis, efficiencies in the range 15–20% seem feasible, even though optimization was not the aim of this work.

A flame-sheet chemistry model and a realistic, specifically developed, one-step Arrhenius kinetics are used and compared in order to assess the importance of finite-rate chemistry effects. Finite-rate is found to play a significant role especially near the extinction limit(low velocities) and at high temperatures (high velocities) where distributed reaction effects are significant and can lead to autoignition.

It has been found that this combustor operation is very sensitive to the equivalence ratio $\phi$ and to the heat exchange parameters. In particular, the most interesting regimes with higher potential efficiency in the energy conversion were found for lean flames. From these operation conditions, increasing $\phi$ or reducing the external heat losses leads to an increase in flame propagation velocity that allows the flame to be stabilized far from the origin, which produces paradoxically higher heat losses and therefore lower efficiency. Typically, for a given burner with fixed external heat losses parameter $h_o$, an optimum $\phi$ exists that produces a maximum efficiency. Reducing heat losses can be used to increase efficiency if the operating equivalence ratio is reduced accordingly for the flame to be stabilized close to the origin, thereby effectively reducing heat losses.

All results shown above are steady solutions of equations (2.1)–(2.18). The unsteady formulation has been used to test, in a non-systematic way, the stability of a few solutions. The results of the stability analysis carried out by Fursenko and Minaev [7] were found to be correct. Furthermore, no oscillatory regime was found and no unsteady extinction–reignition regime, such as FREI [12], could be reproduced.

*Acknowledgements.* This work was supported by projects ENE2015-65852-C2-1-R (MINECO/FEDER,UE), PR2015-00677, BYNV-ua37crdy (Fundación Iberdrola España) and by the Russian Ministry of Education and Science (Grant No. RFMEFI58417X0031).

## References

[1] H. Davy. On the fire-damp of coal mines, and on methods of lighting the mines so as to prevent its explosion. *Phil. Trans. R. Soc. Lond.* **106** (1816) 1–22.

[2] A.H. Epstein, S.D. Senturia, O. Al-Midani, G. Anathasuresh, A. Ayon, K. Breuer, *et al.* Micro-heat engines, gas turbines, and rocket engines the MIT microengine project. In *28th Fluid Dynamics Conference, AIAA-1997-1773* (1997).

[3] A.C. Fernandez-Pello. Micro-power generation using combustion: issues and approaches. In Vol. 29 of *Proc. of the Combustion Institute* (2002) 883–899.

[4] E. Fernández-Tarrazo, A.L. Sánchez, A. Liñán and F.A. Williams. A simple one-step chemistry model for partially premixed hydrocarbon combustion. *Combust. Flame* **147** (2006) 32–38.

[5] K. Fu, D.C. Walther, A.C. Fernandez-Pello, D. Liepmann and K. Miyasaka. Preliminary investigation of a small-scale rotary internal combustion engine. In Western States Section/Combustion Institute; fall meeting (1999).

[6] R.V. Fursenko, S.S. Minaev and V.S. Babkin. Thermal interaction of two flame fronts propagating in channels with opposing gas flows. *Combust. Expl. Shock Waves* **37** (2001) 493–500.

[7] R.V. Fursenko and S.S. Minaev. Flame stability in a system with counterflow heat exchange. *Combust. Expl. Shock Waves* **41** (2005) 133–139.

[8] F.P. Incropera, D.P. DeWitt, T.L. Bergman and A.S. Lavine. Fundamentals of Heat and Mass Transfer 6 edition. John Wiley & Sons Inc (2006).

[9] Y. Ju and K. Maruta. Microscale combustion: technology development and fundamental research. *Prog. Energy Combust. Sci.* **37** (2011) 669–715.

[10] N.S. Kaisare and D.G. Vlachos. A review on microcombustion: fundamentals, devices and applications. *Prog. Energy Combust. Sci.* **38** (2012) 321–359.

[11] K.H. Lee and O.C. Kwon. Studies on a heat recirculating microemitter for a micro thermophotovoltaic system. *Combust. Flame* **153** (2008) 161–172.

[12] K. Maruta, T. Kataoka, N. Kim, S. Minaev and R. Fursenko. Characteristics of combustion in a narrow channel with a temperature gradient. In Vol. 30 of *Proc. of the Combustion Institute* (2005) 2429–2436.

[13] B.J. McBride, S. Gordon and M.A. Reno. Coefficients for Calculating Thermodynamic and Transport Properties of Individual Species. Report TM- 4513, NASA (1993).

[14] S.S. Minaev and E. Fernández-Tarrazo. Microcombustor Analytics. In *Proc. of 14th International Conference on Flow Dynamics, Sendai, Japan* (2017) 190–191.

[15] S.S. Minaev and R.V. Fursenko. Estimates of efficiency of a small-size thermoelectric channel in terms of conversion of heat produced by gas combustion to electric power. *Combust. Expl. Shock Waves* **43** (2007) 384–390.

[16] D.G. Norton, J.A. Federici, T. Bruggemann, K.W. Voit, E.D. Wetzel and D.G. Vlachos. Catalytic micocombustors with integrated thermoelectric elements dor portable power production. *J. Power Sources* **161** (2006) 1469–1478.

[17] D.G. Norton and D.G. Vlachos. A CFD study of propane/air microflame stability. *Combust. Flame* **138** (2004) 97–107.

[18] P.D. Ronney. Analysis of non-adiabatic heat recirculating combustors. *Combust. Flame* **135** (2003) 421–439.

[19] P.D. Ronney. Heat-Recirculating Combustors, in Microscale Combustion and Power Generation. Momentum Press LLC, New York (2015) 287–320.

[20] M. Sánchez-Sanz. Premixed flame extinction in narrow channels with and without heat recirculation. *Combust. Flame* **159** (2012) 3158–3167.

[21] M. Sánchez-Sanz, D. Fernández-Galisteo and V.N. Kurdyumov. Effect of the equivalence ratio, Damköhler number, Lewis number and heat release on the stability of laminar premixed flames in microchannels. *Combust. Flame* **161** (2014) 1282–1293.

[22] I. Schoegl and J.L. Ellzey. Superadiabatic combustion in conducting tubes and heat exchangers of finite length. *Combust. Flame* **151** (2007) 142–159.

[23] M.D. Smooke and V. Giovangigli. Reduced Kinetic Mechanisms and Asymptotic Approximations for Methane-Air Flames, chapter 1: Formulation of the Premixed and Nonpremixed Test Problems. In Vol. 384 of *Lecture Notes in Physics*, Springer-Verlag, Berlin (1991) 1–28.

[24] F.J. Weinberg. A burner for mixtures of very low heat content. *Nature* **251** (1974) 47–49.

[25] Y.B. Zeldovich and D.A. Frank-Kamenetskii. A theory of thermal flame propagation. *Zhurnal Fizichskoi Khimii* **12** (1938) 100–105.